

Politecnico di Milano
Spcecraft Attitude Dynamics
Academic year 2023-2024
Professor: Franco Bernelli Zazzera
Project group n. 12
Project n. 585

Team members			
Person Code	Surname	Name	Bachelor (type and university)
10726940	Bachini	Pier Francesco A.	Aerospace Engineering Politecnico di Milano
10721571	Belletti	Stefano	Aerospace Engineering Politecnico di Milano
10704282	Giardini	Chiara	Aerospace Engineering Politecnico di Milano
10979819	Gómez Sánchez	Carolina	Aeronautical Engineering Universidad Pontificia Bolivariana



POLITECNICO
MILANO 1863

SCUOLA DI INGEGNERIA INDUSTRIALE
E DELL'INFORMAZIONE

Project specifications:

	Assigned specification	Modifications (if any)	Motivation for modification
Platform	minisat (100-500Kg)		
Attitude parameters	Direction cosines		
Mandatory sensor	Magnetic field sensor	Earth horizon sensor	Magnetic sensor only provides attitude determination for 2 axis
Actuators	3 magnetic coils, 1 inertia wheel		

Work distribution:

The workload was evenly distributed among the team members, with sections like Dynamics, Kinematics and Disturbances being built by all team members and compared to minimise the chances of mistakes. The other subsystems were created by multiple people and then tested and validated by all team members.

Contents

1	Introduction	1
1.1	Satellite's Structure	1
1.2	Orbit	2
2	Dynamics and Kinematics	3
2.1	Dynamics	3
2.2	Kinematics	3
3	Environment and Disturbances	4
3.1	Environment	4
3.1.1	Earth magnetic field	4
3.1.2	Orbit propagation	4
3.2	Disturbances	5
3.2.1	Magnetic torque	5
3.2.2	Gravity gradient	5
3.2.3	Atmospheric drag	5
4	Sensors	7
4.1	Choice of components	7
4.1.1	Magnetometer - MAG-3	7
4.1.2	Earth Horizon Sensor - IRES	7
4.2	Sensor modelling	7
4.2.1	Magnetometer	8
4.2.2	Earth horizon sensor	8
5	Attitude Determination	9
5.1	Angular velocity estimation	9
6	Control Law	10
6.1	Detumbling	10
6.2	Nadir pointing	10
7	Actuators	12
7.1	Choice of components	12
7.1.1	Magnetorquers - MT400-2	12
7.1.2	Inertia wheel - RW800	12
7.2	Actuator modelling	12
7.2.1	Inertia wheel	12
7.2.2	Magnetic coils	13
7.3	Actuator control	13
7.3.1	Detumbling	13
7.3.2	Slew and Pointing	13

8 Results	14
8.1 Open loop performances	14
8.1.1 Simulation with no active control	15
8.2 Close loop performances	16
8.2.1 Detumbling	16
8.2.2 Pointing	16
9 Conclusions	19
9.1 Performance analysis	19
9.2 Potential ways to improve the system	19
10 Academic Honesty	20

1 Introduction

The following report focuses on the analysis of the attitude dynamics and control system (ADCS) of a satellite with given design constraints. The goal of the mission is to stabilise the satellite and control it in order to reach an Earth targeting condition. Not all the criteria requested would be the ones picked for a real mission, but the aim of this project is to design, test and present an ADCS that, despite some limitations, is able to provide control to a satellite without adding unnecessary components.

The minimum requirements for the project were the following:

- The satellite must be a minisat (100-500 kg);
- The satellite's attitude must be modelled with direction cosines;
- The satellite must have a magnetic field sensor;
- The satellite must have 3 magnetic coils, and 1 inertial wheel.

An infrared Earth horizon sensor is added in order to satisfy all the objectives of the mission; as will be explained later, this modification to the sensor requirements is a necessary one.

The general scheme of the system is as follows.

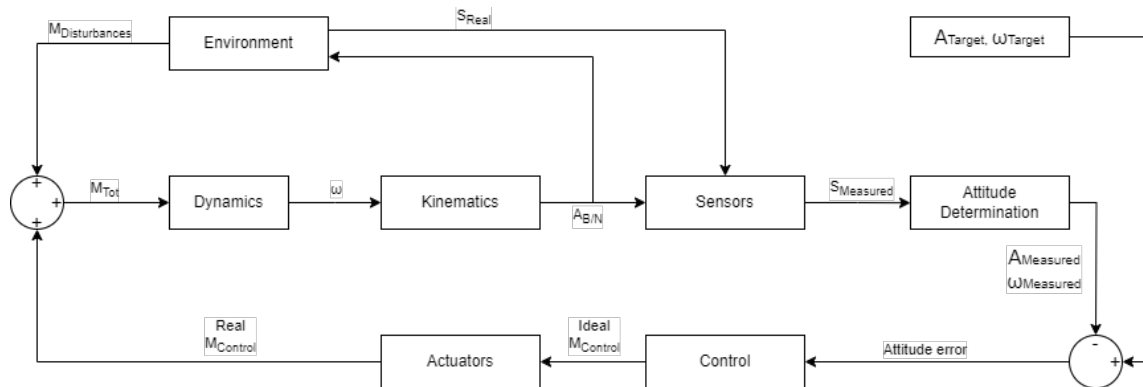


Figure 1: System's schematic

1.1 Satellite's Structure

The structure of the satellite is very important, since it has to sustain launch loads, but also fit the whole mission equipment: sensors, actuators, cables and the actual payload. In the case of this specific mission the satellite has to accommodate:

- 1 inertia wheel (in magenta in Figure 2);
- 1 magnetic field sensor (in green in Figure 2);
- 3 magnetic coils (in blue in Figure 2);
- 1 horizon sensor (in red in Figure 2).

A simplified CAD model of the satellite was designed to verify that all the components are able to fit inside the structure, but also to have an approximated estimation of the inertia moments, reported in Table 1. The dimension were chosen taking into reference the most common minisats in low orbit, and an even mass distribution across the volumes of the object was supposed.

	Mass [kg]	Dimensions [m]
Main body	127	0.8 x 0.8 x 0.886
Single solar panel	4.3	1.2 x 0.8 x 0.02
Total	135.6	
Ixx [kgm ²]	Iyy [kgm ²]	Izz [kgm ²]
23.4677	32.3556	32.9733

Table 1: Characteristics of the satellite

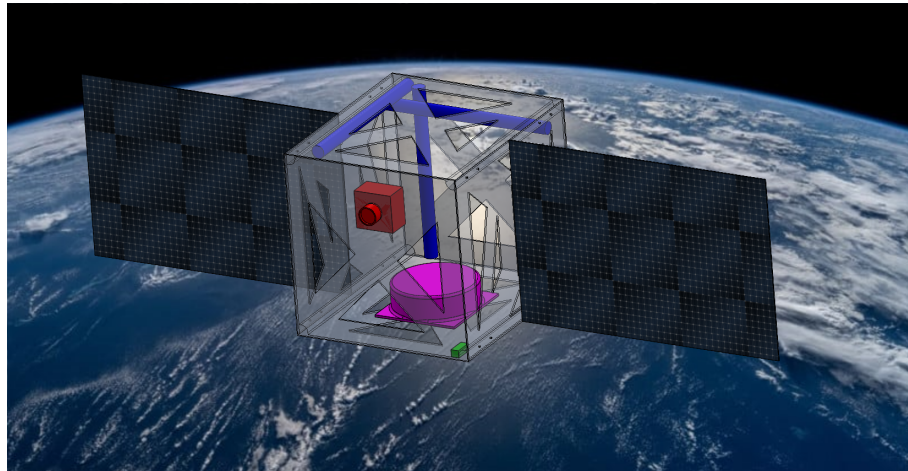


Figure 2: Satellite's CAD model

1.2 Orbit

The orbit chosen for the spacecraft was influenced by the assigned specifications and the mission goal. As both actuators and sensors need to rely on a high enough magnetic field to function properly, a Low Earth Orbit (LEO) was chosen, with the following keplerian elements:

a [km]	e [-]	i [deg]	Ω [deg]	ω [deg]
8016	0.1678	0	0	0

Table 2: Orbital parameters

The orbit is propagated using this parameters in a two-body problem model.

2 Dynamics and Kinematics

2.1 Dynamics

The rotational dynamics of the satellite is described by Euler's equations for a dual spin satellite [1]. The inertia wheel (mounted on the "y-axis") is modelled as spinning at a constant rate, while the changes in angular rate are assumed to be instantaneous.

$$\begin{cases} I_x \dot{\omega}_x + (I_z - I_y) \omega_z \omega_y - I_r \omega_r \omega_y = M_x \\ I_y \dot{\omega}_y + (I_x - I_z) \omega_x \omega_z + I_r \dot{\omega}_r = M_y \\ I_z \dot{\omega}_z + (I_y - I_x) \omega_y \omega_x + I_r \omega_r \omega_x = M_z \\ I_r \dot{\omega}_r = M_r \end{cases} \quad (2.1)$$

Where the terms M_x , M_y and M_z represent the sum of the disturbances and control torques around the satellite's axis and M_r is the torque on the inertia wheel. I_x , I_y , I_z are the principal moments of inertia of the satellites, while I_r is the moment of inertia of the inertia wheel.

2.2 Kinematics

As imposed by the project specifications, attitude modelling is done using direction cosine matrix. Thus, the rotational kinematic of the spacecraft is computed as:

$$\frac{dA(t)}{dt} = -[w \wedge] A(t) \quad (2.2)$$

with

$$[w \wedge] = \begin{bmatrix} 0 & -\omega_z & \omega_y \\ \omega_z & 0 & -\omega_x \\ -\omega_y & \omega_x & 0 \end{bmatrix} \quad (2.3)$$

Where A is the direction cosine matrix that expresses the rotation of the body frame B with respect to the inertial frame N ($A_{B/N}$). As the integration does not preserve the orthonormality of the matrix A , an iterative method has been implemented to ensure it:

$$A_{k+1}(t) = \frac{3}{2}A_k(t) - \frac{1}{2}A_k(t)A_k(t)^T A_k(t) \quad (2.4)$$

As the simulation step is small enough to cause only a small error in the numeric integration, only the first iteration is applied and only when a certain threshold has been reached, in order to save computational power.

3 Environment and Disturbances

3.1 Environment

3.1.1 Earth magnetic field

Because of its internal structure, the Earth generates a magnetic field, which can be approximated using a dipole model. However, since the satellite sensors and actuators closely interact with it and as the orbit is a LEO orbit, a more detailed model is required. The IGRF (*International Geomagnetic Reference Field*) is then used. From the potential function V , the magnetic field \underline{B} can be computed as: $\underline{B} = -\nabla V$, where V is computed as follows:

$$V(r, \theta, \phi) = R_{\oplus} \sum_{n=1}^k \left(\frac{R_{\oplus}}{r} \right)^{n+1} \sum_{m=0}^n (g_n^m \cos(m\phi) + h_n^m \sin(m\phi)) P_n^m(\theta) \quad (3.1)$$

The values of the Gaussian coefficients g_n^m and h_n^m are tabulated, while the Schmidt quasi-normalize Legendre function $P_n^m(\theta)$ and its derivative are calculated through recursive formulas. Finally, looping over the values of n and m , the thirteen order model is computed. To validate the model, it's compared with the IGRF implementation provided by the matlab function *igrfmagm*.

3.1.2 Orbit propagation

The orbit's radius is computed with respect to the origin of an inertial reference frame and its true anomaly in a perifocal reference frame with both frames centred in Earth's centre. As the target angular velocity is based on the value of $\dot{\theta}$, it is calculated as:

$$\dot{\theta} = \frac{n(1 + e \cos(\theta))^2}{(1 - e^2)^{3/2}} \quad (3.2)$$

where n is the average rotational rate of the orbit, while e and a are the orbit's eccentricity and semi-major axis.

The radius of the orbit is then calculated using the two body problem Equation (3.3)

$$\ddot{r} = -\frac{\mu}{r^3} r \quad (3.3)$$

This data is considered to be known to the onboard computer. A 3D representation of the orbit can be seen in Figure 3

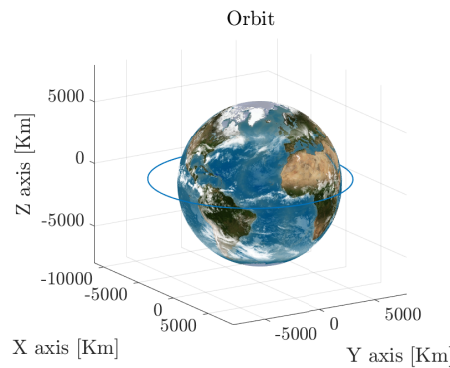


Figure 3: Satellite's orbit

3.2 Disturbances

Any object in space will experience perturbations that will influence its dynamic behaviour. All the models used for external disturbances are described in this section. Using approximated values a preliminary value for maximum torque applied to the spacecraft is computed for each type to compare their effects:

Disturbances	Reference formula	Preliminary max Torque [Nm]	Simulation max Torque [Nm]
Gravity gradient	$M_{max} = \frac{3GM_{\oplus}}{2R_{\oplus}^3} I_{MAX} - I_{min} $	1.9145e-05	1.5575e-05
Solar Radiation Pressure	$M_{max} = P_s A_s (1+q) (c_{ps} - c_g)$	9.4220e-07	—
Magnetic field disturbance	$M_{max} = D_s B_{max}$	2.3798e-06	2.3045e-06
Aerodynamic Drag	$M_{max} = \frac{1}{2} \rho v^2 A_s C_D (c_{pa} - c_g)$	5.4512e-05	5.5924e-05

From the table, only the ones considered more impacting are then modelled.

3.2.1 Magnetic torque

The magnetic torque generated on a spacecraft in orbit around the Earth is the result of the interaction between the external magnetic field and the residual internal dipole of the spacecraft, generated by its electrical and electronic components. Modelling this torque is straightforward, as it can be simply described as the cross product of the internal dipole and the external magnetic field in body frame B :

$$\underline{M}_{mag} = \underline{m} \wedge \underline{b}_B \quad (3.4)$$

with m being the vector of internal dipole, estimated as $\underline{m} = [0.05; 0.05; 0.05] Am^2$.

3.2.2 Gravity gradient

The gravity field is not uniform and depends on the distance from Earth, so since the spacecraft is on a low orbit this leads to a non negligible disturbance torque:

$$\underline{M}_{GG} = \frac{3GM_{\oplus}}{r^3} \begin{bmatrix} (I_z - I_y)c_3c_2 \\ (I_x - I_z)c_1c_3 \\ (I_y - I_x)c_2c_1 \end{bmatrix} \quad (3.5)$$

Where G is the universal gravitational constant, m_{\oplus} is the mass of Earth, r is the distance of the satellite from the centre of Earth, and c_i can be obtained by rotating the vector $[1 \ 0 \ 0]^T$ using the direction cosine matrix $A_{B/L}$.

3.2.3 Atmospheric drag

The atmospheric drag disturbance is given by the interaction between the satellite and upper Earth's atmosphere. Friction between the spacecraft and air particles generates a

disturbing torque perturbing the dynamics of the satellite. The resulting torque can be computed as:

$$\underline{M}_{drag} = \sum_{k=1}^{n_{surfaces}} \underline{r}_k \wedge \underline{F}_{a_k} \quad (3.6)$$

Where \underline{r}_k is the vector connecting the aerodynamic centre of the surface (considered to be coincident with the geometrical centre of the surface) with the centre of mass of the spacecraft. The air drag force is calculated as:

$$\underline{F}_{a_k} = \begin{cases} -\frac{1}{2} C_D \rho(h) v_{rel}^2 \hat{v}_{rel} (\hat{n}_s \cdot \hat{v}_{rel}) A_k & \text{if } \hat{n}_s \cdot \hat{v}_{rel} > 0 \\ 0 & \text{if } \hat{n}_s \cdot \hat{v}_{rel} < 0 \end{cases} \quad (3.7)$$

where $\rho(h)$ is the air density which depends on the altitude of the orbit ($\rho(h) = \rho_0 e^{-\frac{h-h_0}{H}}$), v_{rel} is the relative velocity between the satellite and the atmosphere, C_D is the drag coefficient that is evaluated experimentally and A_k is the area of the surface.

4 Sensors

The only sensor assigned by the projects is a magnetometer. However, using only alone it is impossible to determine the attitude along 3 axis of rotation so, to achieve complete attitude determination, it was necessary to add at least one more type of sensor. The team chose an Earth horizon sensor.

4.1 Choice of components

4.1.1 Magnetometer - MAG-3

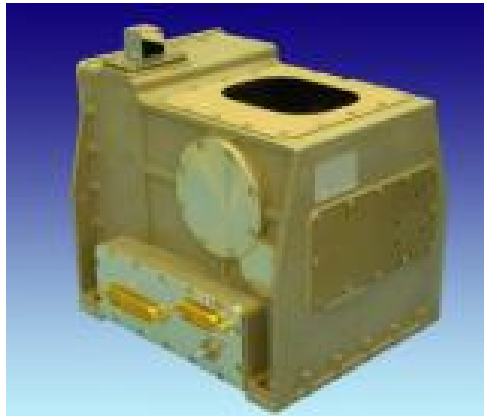
The *AAC SpaceQuest Mag-3* is a 3-axis fluxgate magnetometer, designed to output accurate measures on all three axis and suited for LEO orbits. The main characteristics are [2]:

Dimensions [cm]	Accuracy [%]	Non-linearity [%]	Mass [Kg]
3.51 x 3.23 x 8.26	0.05	0.015	0.1

4.1.2 Earth Horizon Sensor - IRES

The *IRES Infrared Earth Horizon Sensor* is manufactured by the company *LEONARDO AIRBORNE & SPACE SYSTEMS*, capable of providing high accuracy roll and pitch determination. The sensor's specifications are [3]:

Dimensions [cm]	Accuracy [deg]	Update rate [Hz]	Mass [Kg]
16.99 x 16.38 x 15.6	0.05 (3σ)	10	2.5



(a) Earth horizon sensor - IRES



(b) Magnetometer - MAG-3

Figure 4: Sensors

4.2 Sensor modelling

Magnetometer and Earth horizon sensor are modelled using the performance parameters reported in the previous tables.

4.2.1 Magnetometer

The magnetometer can provide the vector of Earth's magnetic field taking also into account an error:

$$\underline{B}_{measured} = e_{linearity} e_{accuracy} \underline{B}_{model} \quad (4.1)$$

where $e_{linearity}$ and $e_{accuracy}$ are the errors given by the data sheet and $\underline{B}_{measured}$ and \underline{B}_{model} are Earth magnetic field vectors measured by the sensor and calculated by the model. A non-orthogonality matrix is also multiplied to simulate the non perfect calibration of the sensor, using the inverse procedure of soft and hard iron calibration, thus transforming the measured data from a sphere to an off-centered ellipse.

4.2.2 Earth horizon sensor

The measurements of the Earth horizon sensor differ from the real ones of an angular error given by the data sheet:

$$\underline{r}_{measured} = \underline{A}_{pitch} \underline{A}_{roll} \underline{r}_{model} \quad (4.2)$$

where \underline{A}_{pitch} and \underline{A}_{roll} are the rotation matrices of the accuracy error on the pitch and roll axes and $\underline{r}_{measured}$ and \underline{r}_{model} are the vectors of the orbit radius in the body reference frame measured by the sensors and computed by the environment model.

5 Attitude Determination

Once the data regarding the position of the satellite with respect to the Earth has been gathered, the next step consists to determine the attitude knowing the information coming from both the sensors and the internal mathematical model. Since the two required sensors complete each other's degrees of freedom, it was not necessary to add any other of them and therefore, having only two measurements, to compute the attitude it was used the triad method. Given two measurements, b_B and r_B and their corresponding directions in inertial space b_N and r_N , the attitude can be obtained as:

$$\begin{aligned} \underline{s}_1 &= \underline{b}_B & \underline{v}_1 &= \underline{b}_N \\ \underline{s}_2 &= \underline{b}_B \wedge \underline{r}_B & \underline{v}_2 &= \underline{b}_N \wedge \underline{r}_N \\ \underline{s}_3 &= \underline{b}_B \wedge \underline{s}_2 & \underline{v}_3 &= \underline{b}_N \wedge \underline{v}_2 \end{aligned} \quad (5.1)$$

By building $\underline{\underline{S}} = [\underline{s}_1 \ \underline{s}_2 \ \underline{s}_3]$ and $\underline{\underline{V}} = [\underline{v}_1 \ \underline{v}_2 \ \underline{v}_3]$ the direction cosine matrix is then obtained:

$$\underline{\underline{A}}_{B/N} = \underline{\underline{S}} \ \underline{\underline{V}}^{-1} = \underline{\underline{S}} \ \underline{\underline{V}}^T \quad (5.2)$$

where \underline{b}_B is the measure given by the magnetometer, \underline{r}_B is the measure provided by the Earth horizon sensor and \underline{b}_N , \underline{r}_N are the respective directions in the inertial frame calculated by the model.

5.1 Angular velocity estimation

The spacecraft angular velocity can be estimated by computing the time derivative of the attitude, weighted by a function, to improve accuracy of the derivation. This, coupled with an effective filtering of the estimated values, can provide an estimation of the angular velocity that can be used for the control in the pointing phase.

6 Control Law

The aim of the control problem is to contrast the effect of the external disturbances, to stabilise the spacecraft during its operative life and execute certain assigned operations.

The control logic is then split in two main phases, each with its own algorithm:

- Detumbling: "B-Dot algorithm" which only requires magnetometer and magnetorquers
- Slew manoeuvre and nadir pointing: Lyapunov function based control algorithm which uses all sensors and actuators on board

6.1 Detumbling

The control logic used to achieve detumbling is based on the B-Dot algorithm: a powerful nonlinear attitude control technique based on magnetorquers as actuators and magnetometers as sensors. The necessary control torque is computed using Equation (6.1), where m is the magnetic dipole generated by the actuators and B is the magnetic field.

$$\underline{M}_c = \underline{m} \wedge \underline{B} \quad (6.1)$$

To calculate the magnetic dipole that needs to be generated, the B-dot bang-bang method is implemented, which uses the maximum possible dipole m_{MAX} that the actuators can generate, multiplied by the sign of the variation of the magnetic field:

$$\underline{m} = -\underline{m}_{max} \operatorname{sign}(\dot{\underline{B}}) \quad (6.2)$$

This phase of the mission is considered concluded after the spacecraft angular velocity norm has been stabilised below 0.01 rad/s .

6.2 Nadir pointing

Due to the close proximity of our orbit with respect to Earth, the goal of the mission is Nadir pointing. To achieve this, a non linear control logic is implemented, based on the Lyapunov function for stability. In this case, no separate algorithm for slew manoeuvring is required, as the control logic aims at keeping the body frame aligned with the target one, while, at the same time, keeping the angular at a target value. Nonetheless, a way to track if the current manoeuvre is slew or pointing is implemented, as it is used to correctly saturate the value of the inertia wheel moment.

To achieve this, the value of the attitude error A_e is checked to be under a certain threshold, chosen as 0.05 rad/s : if the condition is met a counter value is incremented by one, whereas it is reset to zero in the other case. The pointing manoeuvre is executed only when the counter value is above 1000, otherwise the slew manoeuvre is the one happening. This way the inertia wheel can be safely used without leading to overshoot the control moment.

The control moment required according to the Lyapunov function is:

$$\underline{M}_c = -k1 \underline{\omega}_e - k2 (A_e - A_e^T)^V + \underline{\omega} \wedge I \underline{\omega} \quad (6.3)$$

where:

$$\begin{cases} A_e = A_{B/N} A_t^T \\ \omega_e = \omega_t - \omega_B \end{cases} \quad (6.4)$$

and the target quantities are:

$$\begin{cases} A_t = A_{L/N} \\ \omega_t = [0 \ \dot{\theta} \ 0] \end{cases} \quad (6.5)$$

The inverse law to derive the momentum can be used to find the conditions that allow the three actuators to obtain that momentum:

$$\begin{cases} D_x \\ -\dot{h}_y \\ D_z \end{cases} = \frac{1}{B_y} \begin{bmatrix} 0 & 0 & 1 \\ B_x & B_y & B_z \\ -1 & 0 & 0 \end{bmatrix} \begin{cases} M_x \\ M_y \\ M_z \end{cases} \quad (6.6)$$

where $[B_x \ B_y \ B_z]^T$ is the vector of the Earth magnetic field and $[M_x \ M_y \ M_z]^T$ is the vector of the momentum coming from the controller. The conditions found are D_x and D_z the required magnetic dipoles for the 2 magnetic torquers and \dot{h}_y the torque applied on the inertia wheel to obtain the necessary angular velocity.

7 Actuators

The assigned actuators are 3 magnetorquers and 1 inertia wheel.

7.1 Choice of components

The following parts were chosen to be equipped on the satellite.

7.1.1 Magnetorquers - MT400-2

The *MT400-2* magnetic torquers produced by *ZARM Technik AG* assure no potential degradation on orbit and are featured on many satellites, proving their reliability. Their main characteristics are [4]:

Length x Diameter [cm]	Dipole moment [Am ²]	Mass [Kg]
75 x 5.6	0.05	11

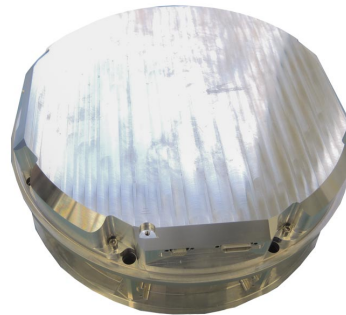
7.1.2 Inertia wheel - RW800

The *RW800* inertia wheel is manufactured by *AstroFein* and its characteristics are as follows [5]:

Dimensions [cm]	Maximum momentum [Nm s]	Maximum torque [Nm]	Mass [Kg]
25x25x10	12	0.2	j=6.0



(a) Magnetic coils



(b) Inertia wheel

7.2 Actuator modelling

7.2.1 Inertia wheel

The inertia wheel changes the dynamics of the satellite from a single spin to a dual spin. Its spin axis is parallel to the satellite's *y* axis and therefore the momentum it generates will only have that one component. It is mainly used during the pointing part of the mission. In order to keep the wheel working, its angular velocity must be kept under the value of the saturation velocity, or it will stop exchanging angular momentum with the spacecraft.

7.2.2 Magnetic coils

Magnetic actuators generate a torque inducing a magnetic dipole in a coil surrounded by a magnetic field:

$$\vec{M} = \vec{D} \wedge \vec{B} \quad (7.1)$$

where \vec{D} is the dipole generated in the coil and \vec{B} is Earth's magnetic field. They are used for both manoeuvres during the mission.

7.3 Actuator control

7.3.1 Detumbling

During the detumbling phase, only magnetorquers are used, as the inertia wheel would not be useful during this part of the mission. As such, the wheel is kept fixed ($h_{wheel} = 0$) while the control torque is calculated as:

$$\underline{M}_c = \underline{m} \wedge \underline{B} \quad (7.2)$$

With the chosen maximum magnetic dipole, the detumbling manoeuvre takes around 6 orbits to bring the angular velocity's norm below 0.01 rad/s .

7.3.2 Slew and Pointing

During this phase of the mission, both magnetorquers and the inertia wheel are used together. Once the control torque has been calculated, the dipole moment D_x and D_z and the wheel contributions \dot{h}_y are computed. This is performed by taking the inverse of:

$$\begin{Bmatrix} M_x \\ M_y \\ M_z \end{Bmatrix} = \begin{bmatrix} 0 & B_z & -B_y \\ -B_z & 0 & B_x \\ B_y & -B_x & 0 \end{bmatrix} \begin{Bmatrix} D_x \\ 0 \\ D_z \end{Bmatrix} + \begin{Bmatrix} 0 \\ -\dot{h}_y \\ 0 \end{Bmatrix} \quad (7.3)$$

which can be computed as:

$$\begin{Bmatrix} D_x \\ -\dot{h}_y \\ D_z \end{Bmatrix} = \frac{1}{B_y} \begin{bmatrix} 0 & 0 & 1 \\ B_x & B_y & B_z \\ -1 & 0 & 0 \end{bmatrix} \begin{Bmatrix} M_x \\ M_y \\ M_z \end{Bmatrix} \quad (7.4)$$

During the slew manoeuvre the integration of $-\dot{h}_y$ starts from a null condition, while during the pointing manoeuvre, it starts from the last value computed during the slew. Moreover, during the slew phase, in order to avoid overshooting and to improve the stability of the control, a lower saturation value of $h_y = h_{ymax}/6$. The magnetorquers don't destabilise the spacecraft, nor lead to overshooting during the manoeuvre, so their maximum dipole is never limited. The control torque is finally computed as can be seen in Equation (7.5) and sent to the dynamics block, closing the whole simulation loop.

$$\underline{T}_c = \underline{B} \wedge \begin{Bmatrix} D_x \\ 0 \\ D_z \end{Bmatrix} + \begin{Bmatrix} 0 \\ -\dot{h}_y \\ 0 \end{Bmatrix} \quad (7.5)$$

8 Results

In this section, the results of the simulation are presented and analyzed.

8.1 Open loop performances

Simulating the system in an open loop configuration, it is possible to assert the perturbations acting on it, as shown in Figure 5

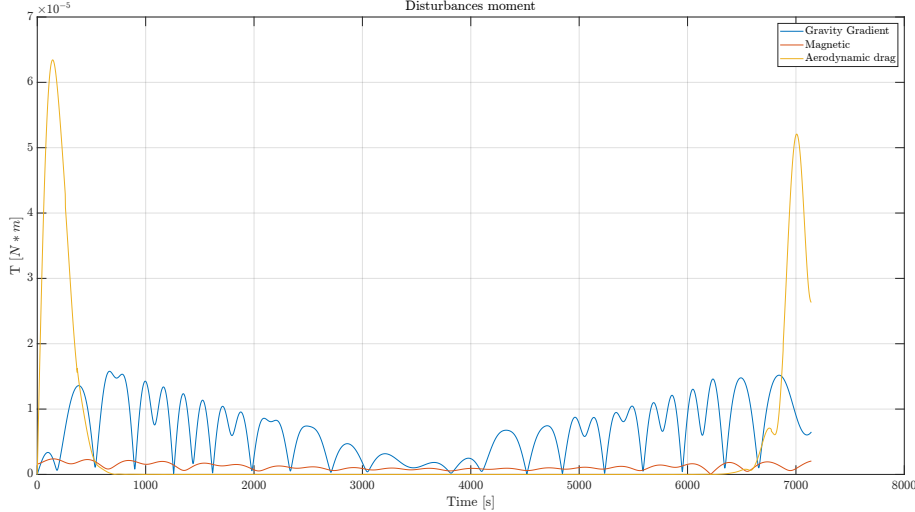


Figure 5: Overall disturbance torque

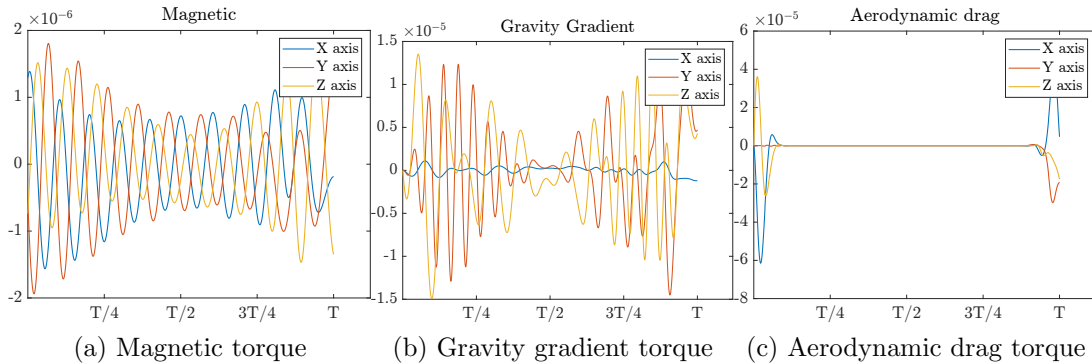


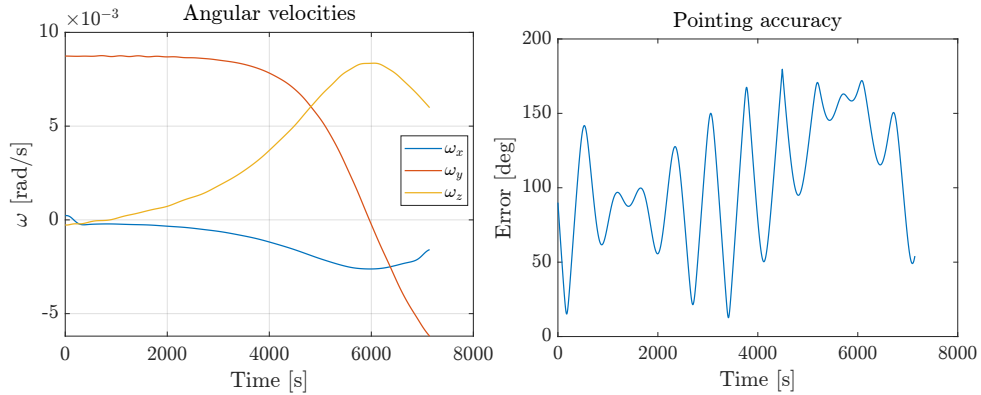
Figure 6: Disturbance torques

The overall disturbance torque is the result of three different perturbations acting on the spacecraft during the mission. Can be seen that, in some parts of the orbit, the perturbation due to aerodynamic drag and gravity gradient are the most prominent ones, but near the apocenter the aerodynamic drag perturbation is almost null and the magnetic one prevails. For this reason, we chose to implement the three perturbations, avoiding the ones which were negligible (i.e. Solar Radiation Pressure). That is a direct consequence of the low altitude of the orbit and the high variation between the maximum and minimum inertia moments of the satellite. It is also possible to notice the position of the spacecraft along the orbit and its orientation affect the perturbation values. From Figure 6 it is also

possible to notice the periodic trend in time of the torques: this is due to the fact that all three effects are related to the altitude, they are higher in the proximity of pericenter and reach a minimum in the apocenter.

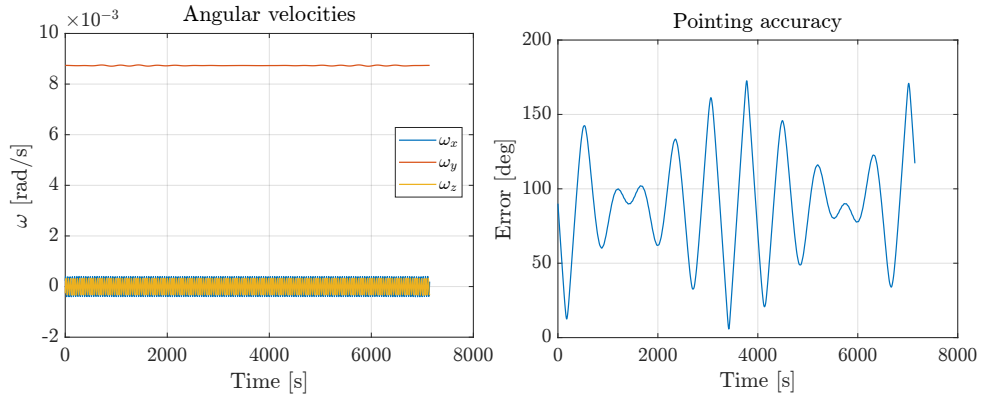
8.1.1 Simulation with no active control

Setting the initial conditions to be the ones achieved during the pointing mission and disabling all control acting on the spacecraft is it possible to analyse how the perturbations affect the satellite.



As it can be seen, the effect of the perturbations disrupts the angular velocity of the spacecraft, making it unable to keep a steady rotation, thus unable to complete its pointing mission.

As the satellite is equipped with an inertia wheel, also the case where the wheel spins with a nominal momentum of $h_y = 4Nms$ can be analysed.



In this case, the wheel provides stability for the spacecraft, making it more resilient to external disturbances. As expected, the satellite keeps a steady angular velocity along the wheel axis, while stabilising and keeping to a lower value the angular velocity on the other two axes.

Note that in both cases, the pointing accuracy, defined as the angular distance of z_B to the nadir direction, is not kept constant proving the need for active control to correctly orient the satellite.

8.2 Close loop performances

As seen in the previous section, the spacecraft is not able to complete its mission without a proper control algorithm.

8.2.1 Detumbling

The first phase of the mission is the detumbling, for which an initial condition of $\omega = [7.5 \ 7.5 \ 7.5] \text{deg/s}$ was chosen. Thanks to B-dot method, the control is able to bring the spacecraft to a slow rotation, as the simulation runs until the norm of the angular velocity below 0.01rad/s . As it can be seen in Figure 7, in total it takes about 6 orbits to achieve this result.

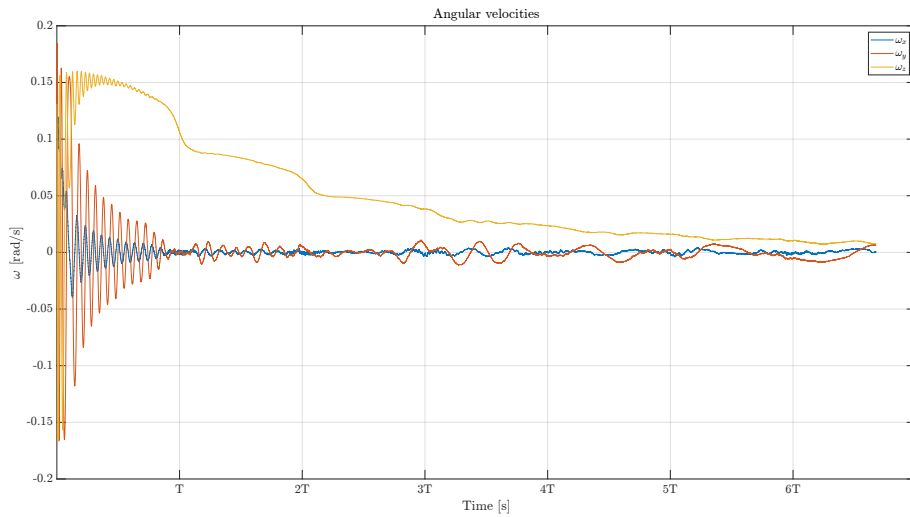


Figure 7: Angular velocities during detumbling

8.2.2 Pointing

Once the detumbling phase is completed, the spacecraft starts Nadir pointing. The objective is to keep angular velocity and attitude under control. Analysing the entire duration of this phase, shown in Figure 8 it is possible to notice how the control takes some time to bring the satellite to the target values:

After the first orbit, however, the correct condition is achieved and the errors are reduced to a minimum value. As it can be seen in Figure 9, the angular velocity on the y-axis perfectly matches the expected value of $\dot{\theta}$, while the other two values are close to zero. At the same time, the pointing accuracy (calculated as the angular distance of z_B to the nadir direction) is kept under a 1° error.

To achieve this precise control on the angular velocity, a good estimation of it is needed. As shown in Figure 10, the error between the real value of ω and the estimated one is in the order of $0.5 * 10^{-3}$. This is particularly relevant during the slew and pointing phase, as the control logic is required to keep a target angular velocity during this phase of the mission. This could be improved with the addition of a gyroscope, which directly measures the angular velocity of the spacecraft, without relying on the attitude determination process, whose result is affected by the noise of the sensors.

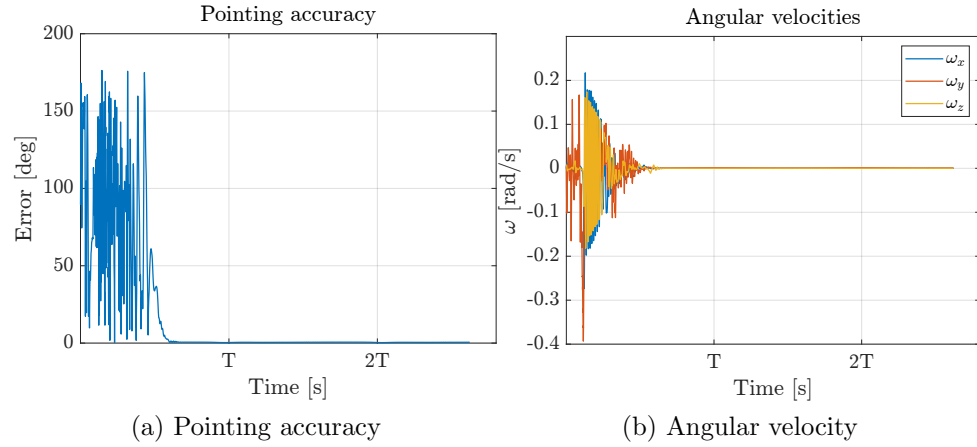


Figure 8: Performance during slew and Pointing

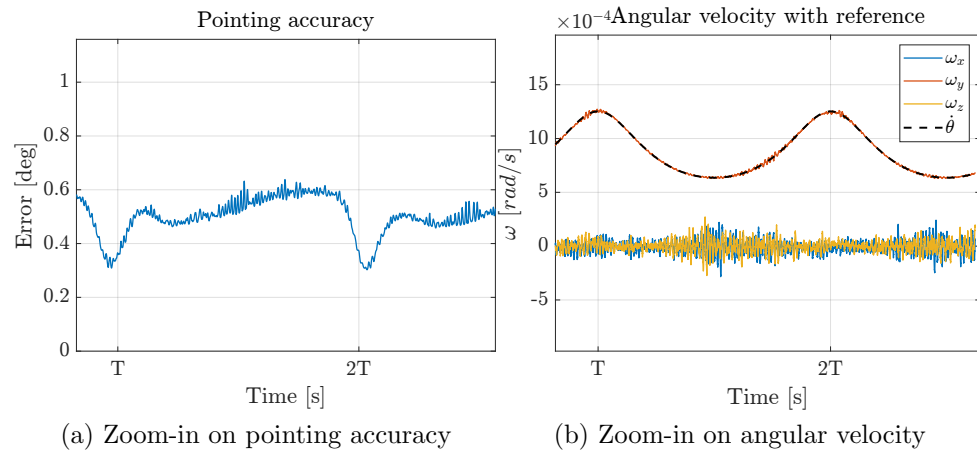


Figure 9: Performance during pointing

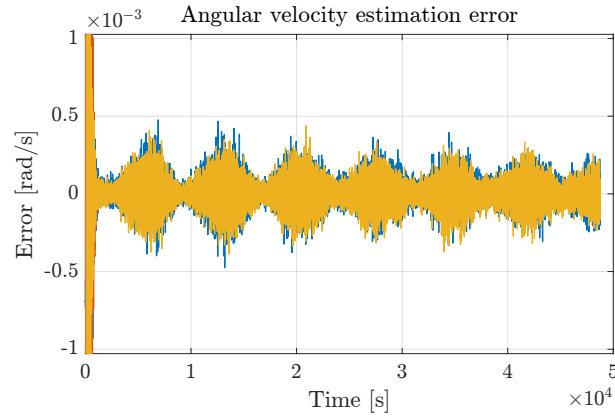


Figure 10: Error in ω estimation

Finally, an analysis on the actuators can also be done. In Figure 11 a comparison between the torque requested by the control algorithm and the one provided by the actuators is shown. As expected, in the beginning of the control operation, the required torque is high. This leads to saturation of both magnetorquers and inertia wheel. Once

the satellite has settled around its target condition the requested torque lowers. Looking at the control torque generated by the two type of actuators, it can be clearly seen how the inertia wheel contribution is prominent during the slew phase, whereas the magnetorquers prevail once the target condition has been acquired and only smaller adjustments are needed.

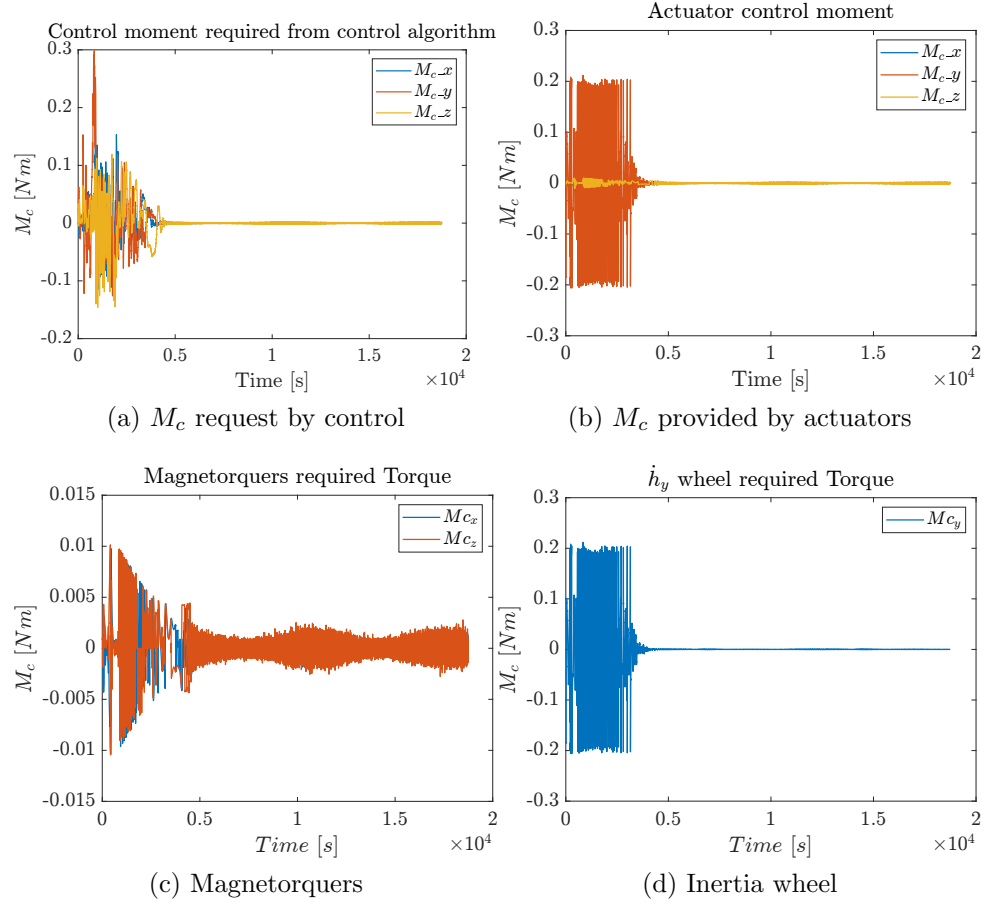


Figure 11: Control moments comparison

9 Conclusions

9.1 Performance analysis

From the data, it emerges that the pointing precision achieved with the system is quite high, in the order of $\sim 0.5 \text{ deg}$ during the Nadir pointing phase. This proves that both the sensor and attitude determination system, as well as the control and actuator logic, can keep the spacecraft stable during the mission.

The presence of the inertia wheel, granting the dual spin stability of the satellite, helps keeping the correct angular velocity, but at the same time it creates a risk of overshooting during the slew manoeuvre and thus has to be carefully balanced using different saturation levels.

Another important aspect to notice regards the the angular velocity determination: while the difference between the real one and the estimated one is in the order of 0.5×10^{-3} , the target one is in the order of 10^{-4} , meaning that the relative error is quite high during this phase of the mission. This is due to the fact that the ω is not measured by onboard gyroscopes, but is estimated using a derivation of the determined attitude and than a filter to remove unwanted noise given by sensors inaccuracies. This makes the estimation particularly unreliable in case of highly varying angular velocities. However, its contribution is still critical to provide an efficient control and the ability to achieve detumbling without needing it (the B-dot algorithm only uses the magnetometer sensor), makes it possible to achieve a good enough estimation during the pointing phase.

9.2 Potential ways to improve the system

On a real satellite, multiple type of sensors would be used, to improve the quality of the attitude determination and, as explained before, to achieve a good estimation of the angular velocity, without derivation and excessive filtering.

Moreover, the use of magnetorquers requires the satellite to be in a low altitude orbit and the satellite to be as light as possible in order to achieve proper control. Depending on the type of mission, other actuators could be added, in such a way that during the slew manoeuvre, where bigger adjustments are needed, this can be used (instead of relying only on magnetorquers).

10 Academic Honesty

Earth's flat image used for 3d representations and animations was downloaded from [Nasa website](#) as there's no restrictions under "[Still Images, Audio Recordings, Video, and Related Computer Files for Non-Commercial Use](#)" for our use. We do not own this image: NASA/Goddard Space Flight Center Scientific Visualization Studio The Blue Marble Next Generation data is courtesy of Reto Stockli (NASA/GSFC) and NASA's Earth Observatory.

The images for both sensors and actuators were taken from their respective datasheets. We do not own these images.

Moreover we did not use any external package other than stock MatLab® and Simulink install.

References

- [1] Franco Bernelli. *Lecture Notes for Spacecraft Attitude Dynamics and Control course*.
- [2] AAAC Clyde Space. www.aac-clyde.space/what-we-do/space-products-components/adcs/mag-3.
- [3] Leonardo Airborne. <https://www.electronics.leonardo.com/it/products/iress-1>.
- [4] Zarm Technik. www.satcatalog.com/component/mt400-2/. MT400-2.
- [5] Astrofein. www.astrofein.com/en/reaction-wheels/rw800/. RW800.